46th AIAA/ASME/SAE/ASEE Joint Propulsion Conference & Exhibit
25 - 28 July 2010, Nashville, TN

AIAA 2010-7040

Detonation Engine Performance Comparison Using First and Second Law Analyses

Eric M. Braun,* Frank K. Lu,† Donald R. Wilson‡
University of Texas at Arlington, Arlington, Texas, 76019
and
José A. Camberos§
U.S. Air Force Research Laboratory, Wright–Patterson Air Force Base, Ohio, 45433

A performance comparison between airbreathing pulsed detonation engine (PDE) and rotating detonation wave engine (RDWE) concepts is made. The flight speed range used for the analysis is approximately Mach 1–5, which is typically thought to be where these concepts are viable and perhaps competitive with each other and Brayton cycle engines. Since the RDWE is ideally capable of operation with a steady state inlet and nozzle, a PDE model with similar steady state systems was developed. The comparison shows a PDE is more efficient at low supersonic speeds, but the relative RDWE performance gradually increases until it becomes comparable. The thermodynamic cycles of these detonation-based engines have been examined in detail using the Second Law to show the losses associated with mixing and purging. Additionally, the combination of an exergy analysis with First Law performance benchmarks proves to be a useful approach for optimization since sources of losses and component interrelationships are easier to identify.

Nomenclature

A	Area
B	Entrance blockage factor
CJ	Chapman-Jouguet property
d	Diameter
c_p	Constant pressure heat capacity
f	Fuel/air ratio
h_{PR}	Fuel heating value
I_{sp}	Specific impulse
L	Detonation tube length
M	Mach number
$\dot{m}_p$	Fuel mass flow rate
PDE	Pulsed detonation engine
q	Dynamic pressure
RDWE	Rotating detonation wave engine
S	Entropy
Sa	Stream thrust function
T	Temperature
V	Velocity

*Graduate Research Associate, Aerodynamics Research Center, Department of Mechanical and Aerospace Engineering, Box 19018. Student Member AIAA.
†Professor and Director, Aerodynamics Research Center, Department of Mechanical and Aerospace Engineering, Box 19018. Associate Fellow AIAA.
‡Professor, Aerodynamics Research Center, Department of Mechanical and Aerospace Engineering, Box 19018. Associate Fellow AIAA.
§Assistant to the Chief Scientist, Air Vehicles Directorate. Associate Fellow AIAA.

η	First Law-based efficiency
ρ	Density
τ	Detonation cycle time
Ψ	Cycle static temperature ratio

Subscripts

0	Freestream property
t	Stagnation property

I. Introduction

THE the design of modern high-performance aircraft requires the collaboration of technical disciplines that have previously operated with some degree of independence. For instance, the wing and body aerodynamics of a subsonic aircraft can be designed around a pre-existing propulsion system and vice versa. This process becomes more troublesome at high flight speeds where the engine inlet and exhaust geometry have considerable effect on the overall aircraft aerodynamics. To assist with optimization around these complex relationships, a need exists for performance metrics with a broader range of application. One proposed metric that has been used extensively in other industries is the exergy analysis method,[1] whereby all losses to aircraft can be quantified using entropy and the Second Law of thermodynamics.[2,3] Exergy (also known as availability) analysis can be used to maximize the work output of aircraft over the varied conditions in a total mission. It can also be described as a method to minimize entropy production of a cycle. Historically, a First Law cycle analysis approach of the engine based on static enthalpy is usually used for missions in conjunction with a metric like minimum takeoff weight. This approach works well for Brayton cycle engines. Performance metrics derived from the First Law, especially efficiencies, tend to focus on a single device as part of the overall system. Since aircraft engines are composed of work-producing and work-consuming devices where these metrics may be defined differently for nontraditional concepts, other metrics using the Second Law can be utilized to level the comparison. Several combined work potential and exergy analysis metrics have been developed for aerospace applications.[4–6] Tracking entropy generation and applying exergy analysis can assist First Law metrics in determining which designs are physically realizable.[7,8]

Emphasis has long been placed on the development of new engines that can bridge the performance gap to scramjet design space, and an exergy analysis may be beneficial for analyzing performance trends and making comparisons. Pulsed detonation engines (PDEs) and rotating detonation wave engines (RDWEs) have temporal dependencies and intra-component relationships with the detonation wave that an exergy analysis can more clearly depict. Both concepts could possibly be used individually or with a hybrid system to reach a hypersonic flight speed. Thus, First and Second Law analyses are applied to these detonation-based engines for two purposes. First, an airbreathing RDWE model has recently been developed,[9] and its performance is compared to a PDE because they may have similar applications. The second purpose is to explore if an exergy analysis is advantageous when combined with a First Law based approach to show temporal effects and other component interrelationships with the detonation wave. Analytical models for the PDE and RDWE are used for this study.

A. Entropy, Work, and Detonation Engine Cycles

The cycle analysis procedure in the current work, immediately evident in the T–s diagrams, differs from previous literature and is outlined in this section. Despite the fact that detonation engines may be either pulsed or continuous, an airbreathing cycle will consist of the following stages: low to moderate compression of the air entering the engine, mixing with fuel, additional compression by a shock wave immediately followed by heat addition, and finally expansion. In a T–s diagram for an ideal Brayton cycle analysis, heat addition at constant pressure is presumed to start immediately after the air passes through the compressor. The fuel and air must mix and thus produce a change in entropy before combustion, but the process is not evident in an ideal Brayton cycle T–s diagram (although mixing losses can be taken into account in the definition of the combustor pressure ratio). However, the PDE and RDWE cycles in this study both have specific times when the fuel and air mixture is present in the engine after compression and before detonation. As shown by Petela, exergy losses can be split between the shock wave compression and heat addition processes of the detonation wave itself.[10] When applied to an engine with an inlet system, splitting the exergy losses (or

entropy increase) while including mixing can provide further insight into the sources of detonation engine thermodynamic losses.

Figure 1 shows Brayton cycle T–s and p–ν diagrams as calculated for an uninstalled engine in Ref. 11. For this procedure, a stoichiometric mixture of H_2–air is used with $\Psi = 2$, $M_0 = 3.0$, $q_0 = 2000$ lbf/ft^2, $T_0 = 216.7$ K, and ideal component performance. The area enclosed by the diagrams can be integrated to determine specific work. Since fuel mixing and combustion both occur in Fig. 1(b) between states 3 and 4 at constant pressure, no change in work would occur upon integration while accounting for mixing.

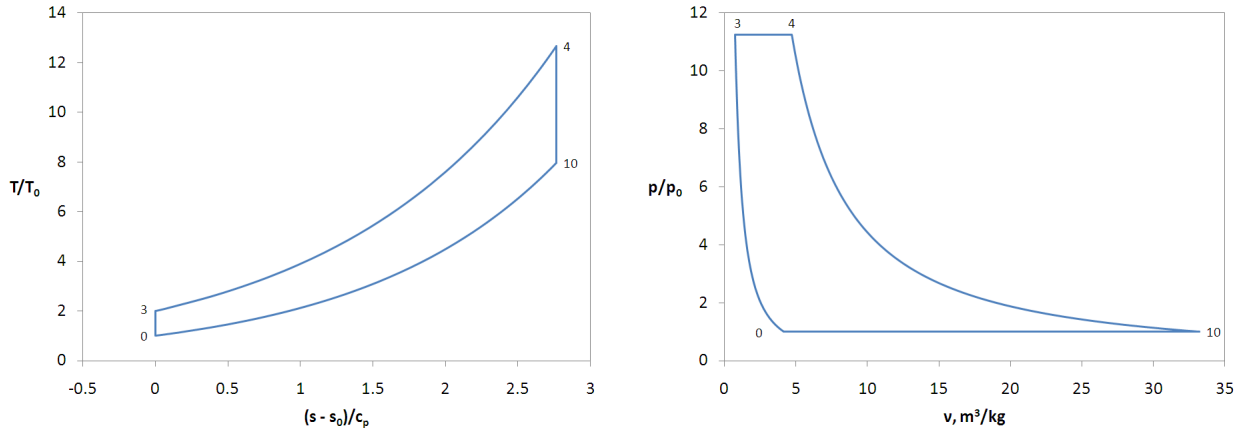

(a) T–s diagram.

(b) p–ν diagram.

Figure 1. Ideal Brayton cycle analysis example for an airbreathing engine.

The T–s and p–ν diagrams can also be created for a detonation-based cycle. For an ideal analysis, the compression from the inlet system is considered as an isentropic process, but additional compression from the shock wave is associated with an entropy increase. Heat addition generates additional entropy while the expansion process is isentropic. The detonation-based cycle analyses in this study are integrated with the chemical kinetics program Cantera[12] which, when combined with additional software libraries,[13] can calculate the thermodynamic state changes for the detonation wave.

In Fig. 2(a), the T–s diagram includes a stage labeled 3m. This stage accounts for the entropy increase due to the addition of H_2 to the air from the compressor. Assuming the fuel is injected at the same temperature and pressure as the air from the compressor, T/T_0 remains constant while entropy increases. The shock wave from the detonation process then moves the flow to the ZND point, followed by heat addition to the CJ point at stage 4. In this diagram, S_0 must account for the hydrogen injection as shown in Eq. 1.

$$S_0 = \frac{f S_{H_2}\left(T_3, p_3\right) + S_{air}\left(T_0, p_0\right)}{1 + f} \tag{1}$$

A horizontal line is also formed in the corresponding p–ν diagram occurs at constant static pressure. In this diagram, chemical non-equilibrium has been accounted for between stages 3m→4. An inert Hugoniot curve starting at stage 3 does not match with the ZND point. Instead, a H_2–air Hugoniot curve is created with variable γ using Eq. 2.

$$\frac{p}{p_3} = \frac{1 + \gamma - (\gamma - 1)\,\frac{\nu}{\nu_3}}{1 - \gamma + (\gamma - 1)\,\frac{\nu}{\nu_3}} \tag{2}$$

Note that the ν axis on the p–ν diagram stops at 5 m^3/kg to zoom in on the changes to p/p_0. For this H_2–air cycle, $\nu_0 = 4.14$ m^3/kg and $\nu_{10} = 27.25$ m^3/kg. The importance of accounting for mixing in these diagrams lies with the fact that they can be integrated to solve for work. With no consideration for mixing, there is a tendency to move from stage 3 to ZND which would result in an overestimation of work upon integration. This overestimation occurs to a lesser extent with hydrocarbon–air mixtures. The entropy rise due to mixing is still noticeable in Fig. 2(c), but the similarity in specific volume of air and methane does not significantly alter the p–ν diagram. Presumably, the addition of heavier fuels will result in a movement to the left on the p–ν diagram between stages 3→3m.

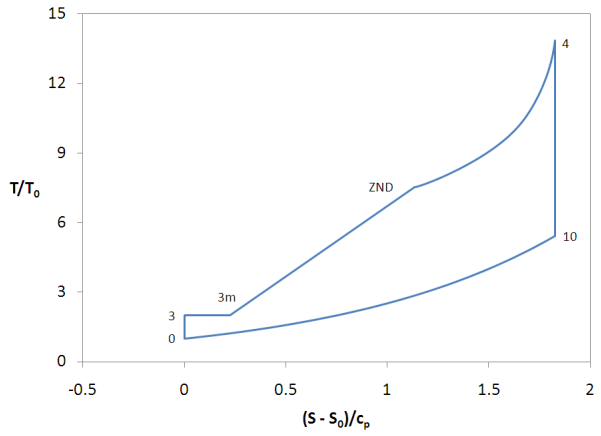

(a) H_2–air T–s diagram.

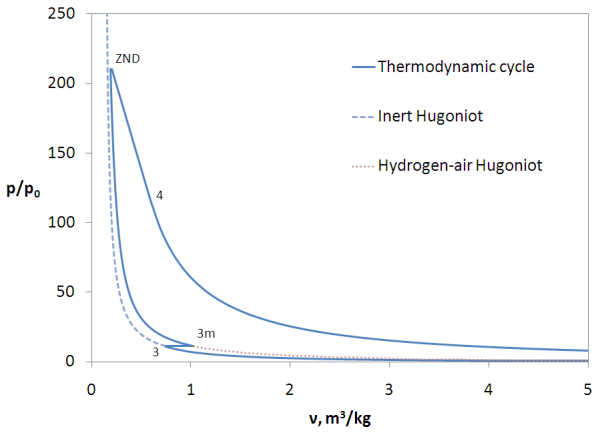

(b) H_2–air p–ν diagram.

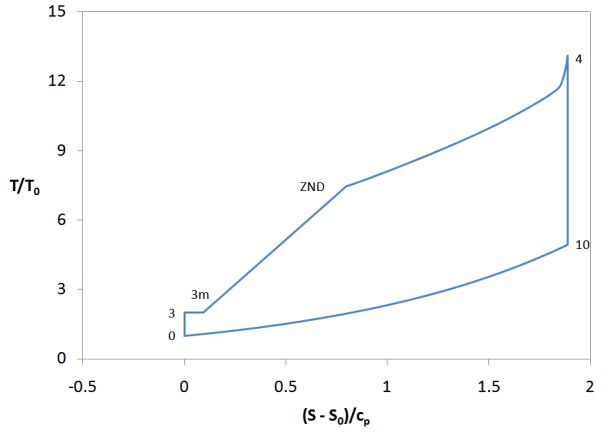

(c) CH_2–air T–s diagram.

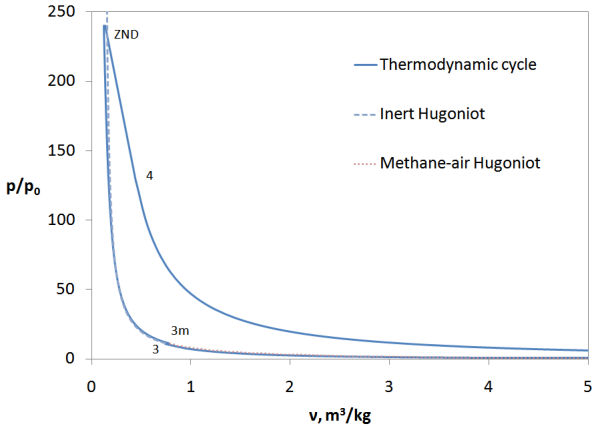

(d) CH_4–air p–ν diagram.

Figure 2. Detonation cycle analysis example for an airbreathing engine.

II. Rotating Detonation Wave Engine

The development of the analytical model for the airbreathing RDWE is described in detail in Ref. 9 and summarized in this section. Rocket-mode RDWEs have been experimentally developed over the course of several decades, with results summarized by Bykovskii et al.[14] Due to the high frequency of the rotating wave, an airbreathing RDWE has the potential for a steady inlet and nozzle without the need for a complex valve system that may be necessary for a steady PDE. The steady RDWE inlet system contains an isolator which delivers air axially into the detonation annulus. Figure 3 shows an unwrapped view where the air entering the annulus is colored in a light blue region. In the figure, fuel is added from an injection system mounted in the annulus. The axial height of the detonation wave is determined by the velocity of the incoming air, the diameter of the annulus, and the velocity of the detonation wave (V_{CJ}). This height is split into h and h_{csb}, which account for the reactive mixture and a portion that burns before the detonation wave due to interaction with hot products from the previous rotation. A model for detonation wave properties in a constant area tube was modified for a two-dimensional expansion, which creates the attached oblique shock as the expanding products interact with the previous wave products. Air may again enter the annulus when the products under the oblique shock expand back to the original inlet pressure.

To ensure stability, the inlet pressure is matched in a convergence process with the average annulus pressure by increasing the ratio of the detonation channel area to that of the isolator. Assuming the isolator flow is supersonic, the area increase reduces the annulus static pressure and increases the axial velocity. Such a technique results in a performance loss, but the pressure gain from the detonation wave cannot be counteracted by any mechanical means. The annulus property distributions are then averaged using

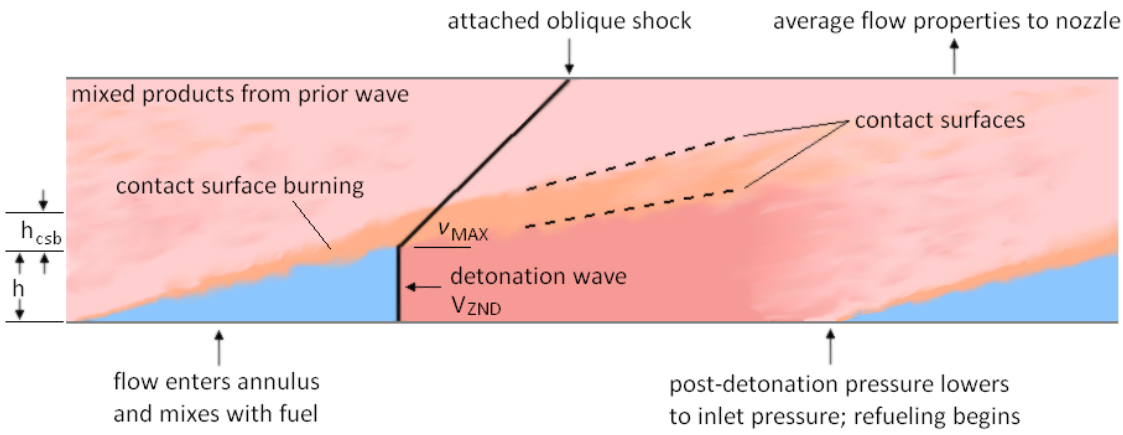

Figure 3. Schematic of the rotating detonation wave structure.[9]

isentropic relations before the products are exhausted through a nozzle. Despite the loss in performance due to the area increase, the specific impulse of an ideal RDWE still can reach over 4000 s with a flight speed up to about Mach 5.0. In the T–s diagram of Fig. 4(b), stage 2 matches stage 3 from Fig. 2(a). The RDWE stage 3 then accounts for the area expansion, and mixing with hydrogen is again labeled stage 3m. Unlike the ideal PDE model of Fig. 2(a), the detonation products mix together and are averaged in stage 5 prior to the nozzle.

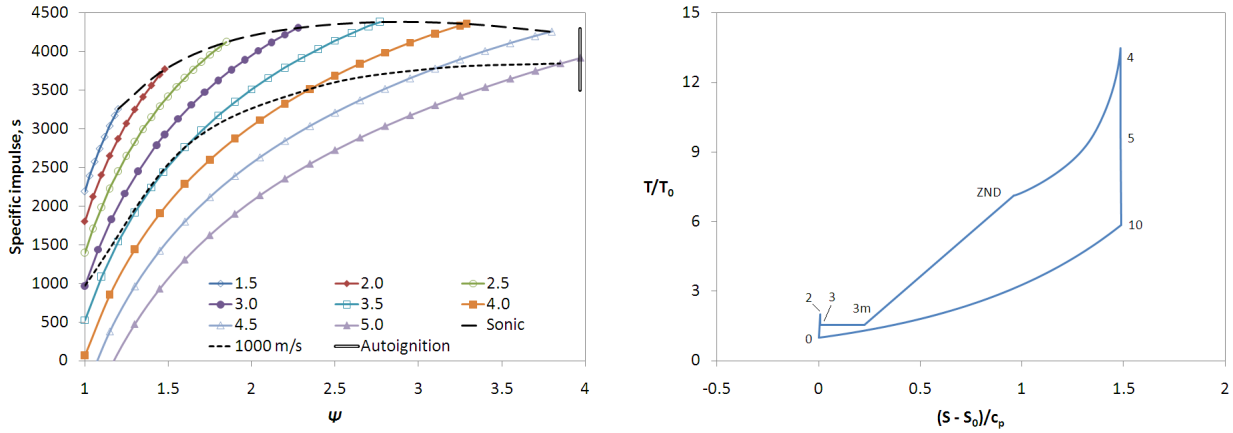

(a) Specific impulse.[9]

(b) T–s diagram for $M_0 = 3.0$ and $\Psi = 2.0$.

Figure 4. Performance versus cycle static temperature ratio for an ideal RDWE with $q_0 = 95$ kN/m^2, $T_0 = 216.7$ K, $d = 0.5$ m, H_2–air, and no contact surface burning.

III. Pulsed Detonation Engine

The pulsed detonation model detailed in this section was created to have similar components as the RDWE to facilitate the comparison. Chiefly, these components are a steady-state inlet, an isolator coupled with a plenum chamber, and a steady-state nozzle. A variety of PDE concepts have dealt with the prospect of integrating a steady-state inlet system. Matching the inlet with the detonation tube(s) has indeed been considered to be one of the more difficult issues to mitigate for PDEs.[15] Since the entrance to the detonation tube itself must be closed off during part of the cycle, instabilities can exist in the inlet system. Consequently, an inlet connected to the detonation tube via a constant area channel is probably not feasible because the engine would unstart with every cycle. For a single-tube PDE, an analysis was conducted with the tube coupled to a plenum chamber to ensure pressure transients would not unstart the engine.[16] According

to that study, the plenum chamber will have to be large compared with the tube diameter. Multi-tube studies have similarly assumed an acoustic cavity would be present in front of the tube entrances, where phase-shifting the detonations dampens pressure fluctuations.[17,18] To be similar to the RDWE, this PDE model assumes a steady state inlet system. The inlet is coupled with a plenum chamber connected to a large number of detonation tubes, such that the transient disturbances from them opening and closing are negligible. With a given tube length and filling velocity, a ratio between tubes open for filling and those closed off for detonation can then be calculated. As will be shown, this ratio can then be used to size the plenum chamber. Presumably, the detonation tubes will be arranged in a circular area with a rotating plate or valve to keep the ratio of open tubes to closed tubes constant. In practice for a multi-tube PDE, the products from the individual detonation tubes must mix prior to the nozzle. In Figs. 2(a) and 2(c), the stage 4 products are immediately exhausted through a nozzle to stage 10. For this model, the change in properties due to mixing is accounted for at stage 5. The processes from stage 4→5 and 5→10 are both considered to be isentropic. Similar to the discussion by Heiser and Pratt on the expansion process of a PDE nozzle,[19] mixing and exhaustion from multiple tubes is complex and no simple devices have been constructed that can ensure an isentropic process.

A. Model

For the PDE model, the stage 2 inlet properties are calculated as a function of cycle static temperature ratio Ψ and compression efficiency η_c to compare with the RDWE.[9] While using a theoretical rotating plate that keeps a percentage of the tubes open for filling from the inlet, a control volume analysis can be performed that solves for the area increase required for a plenum chamber. The plenum chamber keeps pressure fluctuations due to the tubes opening and closing from causing an unstart condition, and it keeps the stage 2 and 3 properties equal. The filling area of the tubes is equal to the area of the flow from the inlet system as shown in the schematic of Fig. 5. In Fig. 5, the fraction of the detonation tubes being blocked from filling is denoted by B, so $(1-B)A_3$ is equal to A_2. Each detonation tube then fills with the flow properties from stage 3. The value of B must be found using an interative solution while calculating the time the detonation tube produces useful thrust. A model by Endo and Fujiwara that predicts the thrust wall pressure history during the detonation cycle has been used to model the tubes.[20] Entropy generation is also tracked through each stage of the engine and exergy destruction may be calculated using the Gouy–Stodola theorem.[21] This process is summarized in Eqs. (3)–(5) where the filling time, purge time, and exhaust time are denoted as τ_F, τ_P, and τ_E, respectively. In the convergence process, an initial estimate for B is updated using Eq. (4).

$$\frac{A_3}{A_2} = \frac{1}{1-B} \tag{3}$$

$$B = \frac{\tau_F + \tau_P}{\tau_F + \tau_P + \tau_E} \tag{4}$$

$$\tau_{cycle} = \tau_F + \tau_P + \tau_E \tag{5}$$

Using a specified detonation tube length L, the filling time requirement τ_F can be calculated. An air purge may be added between the filling and detonation portions of the cycle to eliminate contact surface burning between the incoming reactive mixture and detonation products. The purge time τ_P may be varied as a

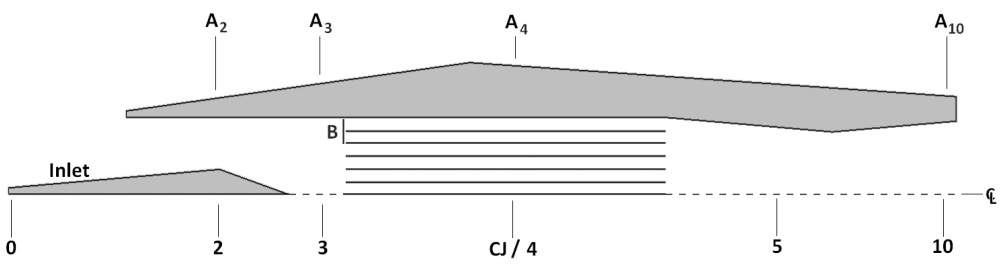

Figure 5. PDE model geometry and stage designations (not to scale).

percentage of the filling time. The exhaust time τ_E is calculated using the model by Endo and Fujiwara.[20] Using the properties of the reactive mixture with fuel added at constant pressure, the model calculates the thrust wall pressure as a function of time. When the thrust wall pressure lowers again to the filling condition, the tube may open again to fill. An iterative solution is needed since the exhaust time is a function of the initial conditions whereby the detonation tube filling fraction must be matched to the exhaust, filling, and purge times.

Although the thrust wall history is captured, the properties at the exit of each individual detonation tube are required for the mixing that occurs at stage 5. As the front of the detonation wave is precisely at the end of the detonation tube, the density distribution across the entire tube can be calculated and then averaged to find the mass of the detonation products. Other properties can be found by using isentropic relations. The average exit velocity is determined using the timing of the cycle components and the conservation of mass equation. In Eq. (6), the velocity is determined using τ_F and τ_E because the remaining detonation products exit the tube at p_3 as the tube refills. The term L/V_{CJ} is subtracted from the timing since τ_E has been formulated to account for the detonation wave propagation time in the tube where products are not exiting. If there is no purge air used in the cycle, $\bar{V}_{det}$ becomes the stage 5 velocity. If a purge is utilized, then Eq. (6) is expanded to include the additional air.

$$\bar{V}_{det} = \frac{\rho_3 V_3 \tau_F}{\bar{\rho}_{det}\left(\tau_F + \tau_E - L/V_{CJ}\right)} \tag{6}$$

Stage 5 is not associated with an area increase. The mixed airflow is also subsonic, so the schematic in Fig. 5 depicts a converging-diverging nozzle. One difficulty that occurs with this model is the average pressure of the detonation products at stage 5 is higher than the inlet pressure p_3. Consequently, the PDE tubes may be difficult to fill once open. Fortunately, a practical airbreathing PDE will operate at high Ψ values where performance is greatest. For the current model, the highest Ψ values associated with a given M_0 usually have p_5/p_3 ratios of 2–4 and a stage 5 Mach number of about 0.25–0.5. As the flow in the converging section of the nozzle accelerates to the sonic speed, the pressure can reduce to a value near p_3. Thus, this model could be practical but designing the geometry and equipment necessary to ensure this process can be isentropic is a complex issue.

Stream thrust-based equations from Ref. 11 are employed for the nozzle as they were with the RDWE.[9] In Eq. 7, the term V_5^2 is usually small when compared with $2c_{p,10}\left(T_5 - T_{10}\right)$. The exit–to–inlet area ratio is determined using the geometry established by the cycle. Although the specific thrust equation is not altered when using purge air, the specific impulse equation must be modified to account for air that enters the engine but is not mixed with fuel.

$$V_{10} = \sqrt{V_5^2 + 2c_{p,10}\left(T_5 - T_{10}\right)} \tag{7}$$

$$\frac{A_{10}}{A_0} = \Psi \frac{p_0}{p_2}\frac{V_0}{V_2}\left(1+f\right)\frac{1}{1-B}\frac{\rho_5 V_5}{\rho_{10} V_{10}} \tag{8}$$

$$\frac{F}{\dot{m}_0} = \left(1+f\right)Sa_{10} - Sa_0 - \frac{R_0 T_0}{V_0}\left(\frac{A_{10}}{A_0} - 1\right) \tag{9}$$

$$I_{sp} = \frac{F/\dot{m}_0}{f g_0}\frac{1}{1+\tau_P/\tau_F} \tag{10}$$

B. Ideal Performance

Figure 6 shows the ideal multi-tube PDE performance results using stoichiometric H_2 and CH_4 fuel/air mixtures. In terms of dimensionless heat addition $\widetilde{q} = f h_{PR}/c_{p,0}T_0$, the H_2 and CH_4 fuels have values of 15.7 and 13.4, respectively. The results from the hydrogen fuel cases are similar to what has been estimated for other ideal PDE studies. However, performance does not continue to slowly increase with Ψ as in other studies because of the reduction in the tube filling velocity. As V_3 decreases, τ_F becomes larger with respect to τ_E. Once V_3 becomes subsonic, τ_F and A_3/A_2 increase rapidly and finally cause specific impulse to drop with Ψ. Like the RDWE performance map, this PDE model has been charted for M_0 up to 5. The Mach 4.5 and 5 cases do not appear to reach a performance maximum before Ψ reaches an autoignition point. The methane PDE performs similarly with a lower I_{sp} as would be expected.

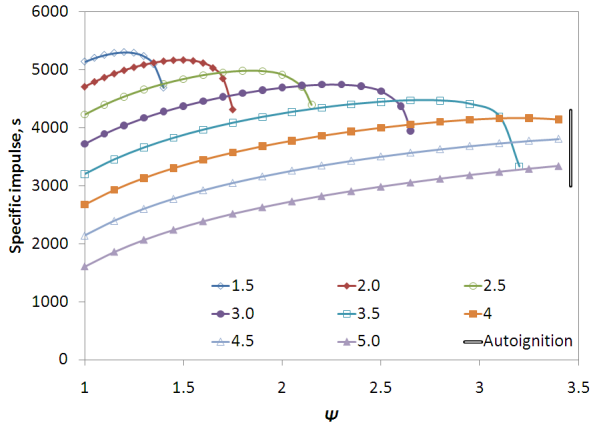

(a) H_2–air specific impulse.

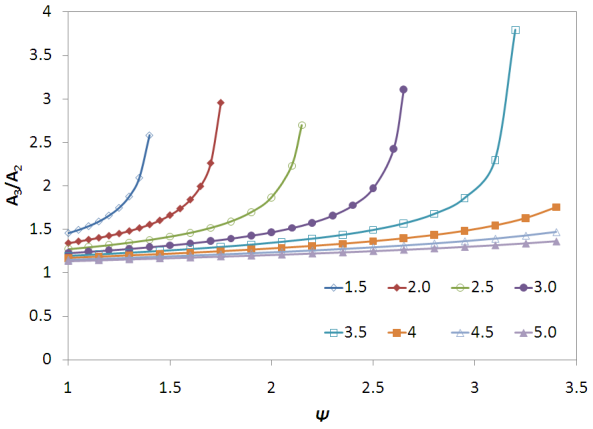

(b) H_2–air plenum area increase.

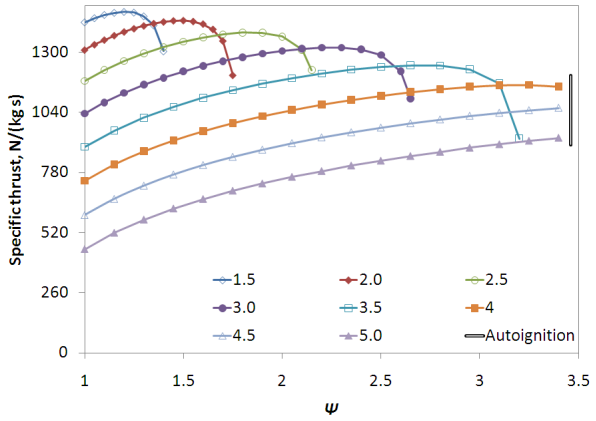

(c) H_2–air specific thrust.

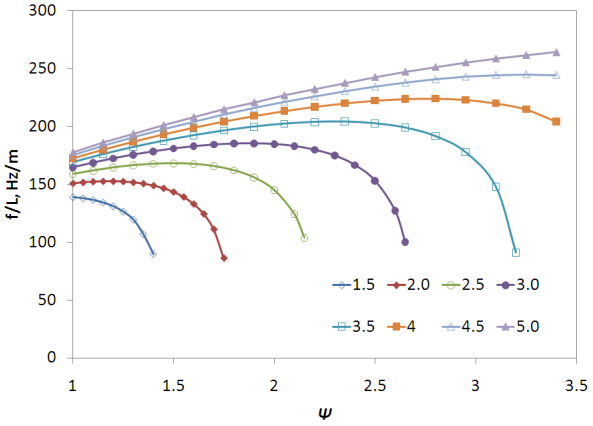

(d) H_2–air tube operating frequency.

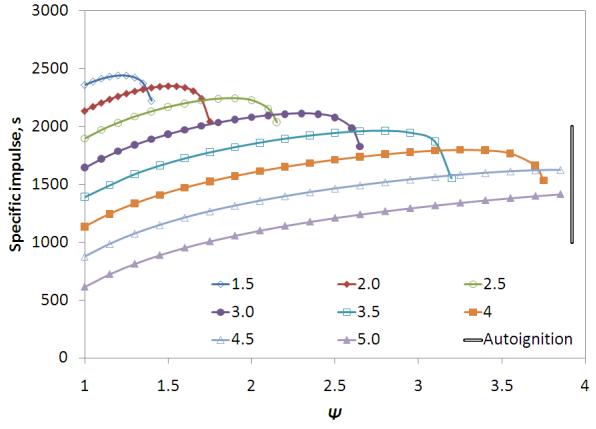

(e) CH_4–air specific impulse.

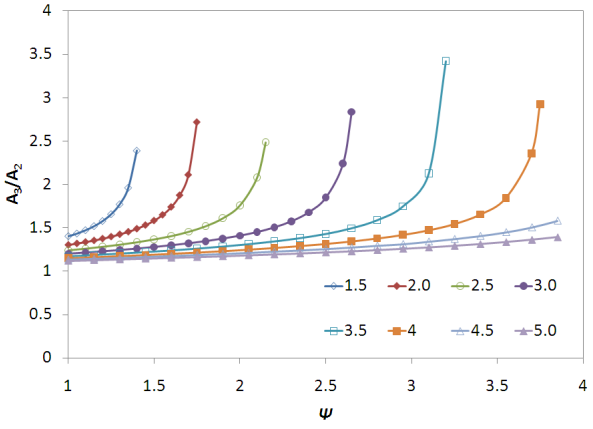

(f) CH_4–air plenum area increase.

Figure 6. Ideal multi-tube PDE model performance versus Ψ with $q_0 = 95$ kN/m^2, $T_0 = 216.7$ K, a one meter tube length, and no purge air. Lines of constant flight Mach number are plotted.

Figure 6(d) shows the operating frequency of the PDE normalized with the length of the detonation tubes, which ranges between 100–250 Hz per meter. For $M_0 = 1.5$, the frequency continues to decrease with Ψ. The CJ pressure ratio decreases with Ψ, which means τ_E will always decrease with Ψ for a given flight speed. Because the CJ pressure ratio is not significantly affected over the Ψ range at Mach 1.5, τ_F controls the trend because it increases as the tube filling velocity decreases. At higher speeds and temperatures, τ_E becomes much greater than τ_F and the frequency continues to rise because the CJ pressure ratio decreases.

C. Effect of Purging

Figure 7(a) shows the effect of adding purge air to the PDE cycle. Three arbitrary cases are charted, one where $M_0 = 2.5$ with $\Psi = 2.0$ and two where $M_0 = 4.0$ with Ψ equal to 2.0 and 3.0. Performance drops since the purge air both reduces overall thrust and increases the plenum area, which increases the last RHS term in Eq. (9). As the fraction of purge air extends beyond 1.0, the specific impulse can drop to 0. Similar to the discussion on accounting for the entropy increase from mixing on a T–s diagram before detonation, the effect of the purge air fraction can also be plotted in the diagram. Figure 7(b) is created using the $M_0 = 3.0$, $\Psi = 2.0$ PDE case. The original path is shown with cases where τ_P/τ_F is 0.1 and 0.3. Equation (11) shows how the reference entropy value S_0 must again be modified since the purge air is referenced to the ambient flight condition.

$$S_0 = \frac{f S_{H_2}(T_3, p_3) + (1 + \tau_P/\tau_F) S_{air}(T_0, p_0)}{(1 + \tau_P/\tau_F) + f} \tag{11}$$

Figure 7(b) indicates separate paths for the purge and detonation gases before they mix at stage 5. As the amount of purge air increases, the dimensionless entropy of the cycle decreases from stage 4→5. This behavior does not violate the Second Law since there is indeed entropy generation greater than or equal to zero from stage 4→5. The loss in entropy of the detonation products from stage 4→5 is matched with the increase in entropy of the purge air from stage 2→5. Mathematically, the entropy balance is expressed as $\dot{m}_{purge}\dot{S}_{purge} + \dot{m}_{det}\dot{S}_{det} = 0$.

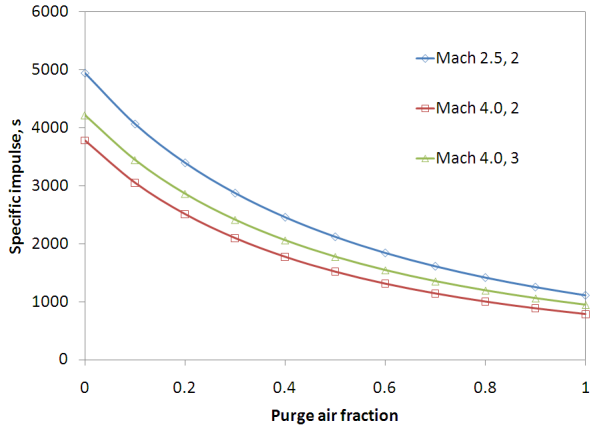

(a) Specific impulse (cases of M_0, Ψ).

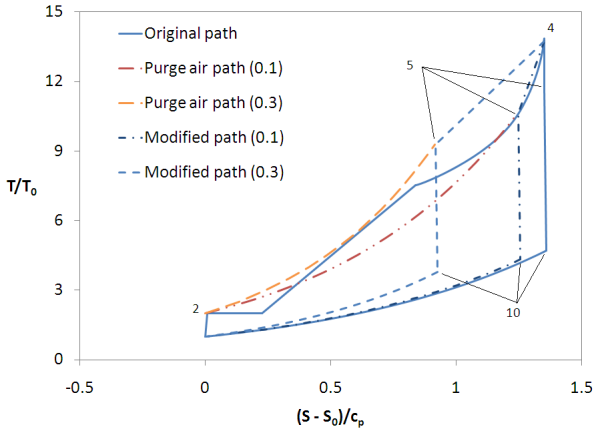

(b) T–s diagram for $M_0 = 3.0$ and $\Psi = 2.0$ with two purge air fractions.

Figure 7. The effect of the purge air fraction on the multi-tube PDE performance.

IV. Cycle Comparisons

This section presents and compares the PDE and RDWE cycles in order to understand their relative performance. First and Second Law performance metrics are employed in the comparison.

A. Specific Impulse and Work

Figure 8 directly compares specific impulse and thrust for the steady-state PDE and RDWE models. Flight Mach numbers of 1.5, 3.0 and 5.0 were used in order to identify the major trends. At all times, the PDE

outperforms the RDWE at low values of Ψ. This trend can be attributed to the fact that the area increase and subsequent performance loss of the RDWE is highest when Ψ is low. The difference in performance is highest when the flight speed decreases. The performance of the RDWE becomes comparable with the PDE as M_0 rises above 3.0. The RDWE eventually outperforms the PDE at high Mach numbers because the performance loss due to the area increase is low.

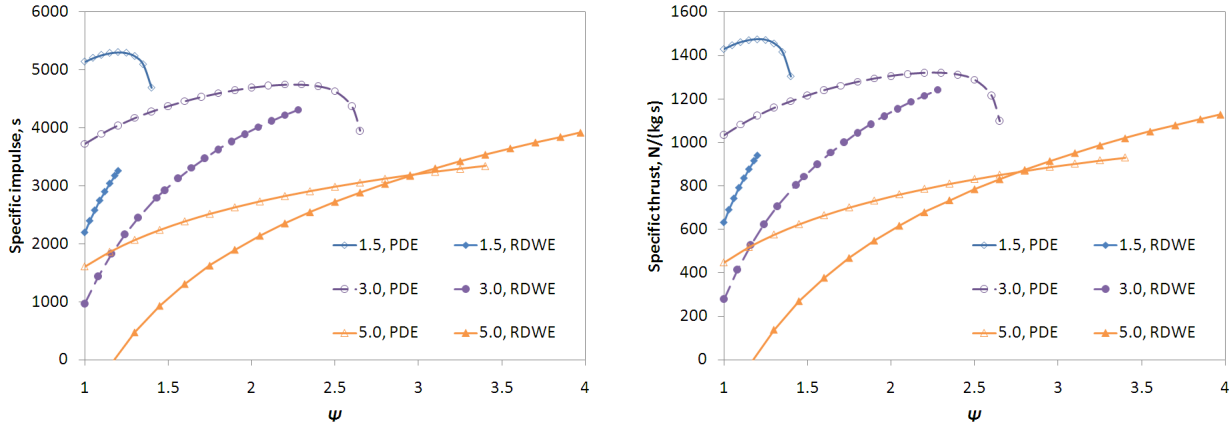

(a) Specific impulse.

(b) Specific thrust.

Figure 8. Performance comparison between the steady-state PDE and RDWE models.

Figure 9 shows a RDWE and PDE performance comparison utilizing T–s diagrams. When a low Mach number is coupled with a low cycle static temperature ratio, Fig. 9(a) shows that one RDWE disadvantage stems from the decrease in temperature from the ambient flight condition. The path of the cycle does not enclose one area as the curve from stage 10→0 ends up above the path from stage 3→3m. This result is not unexpected since the loss of temperature from the ambient condition should produce negative thrust in the engine after stage 3m. For the PDE, the fuel addition results in a minimal amount of thrust generated by stage 3m. Due to the area increase and temperature reduction, the area enclosed by the cycle is significantly less for the RDWE. The RDWE stage 10 temperature ratio is also higher because the pressure at stage 5 is lower and a nozzle is not as beneficial. For the $M_0 = 3.0$ case where Ψ is 2.0, the RDWE performance begins to be more comparable with the PDE as the temperature reduction from stage 2→3 is not as great.

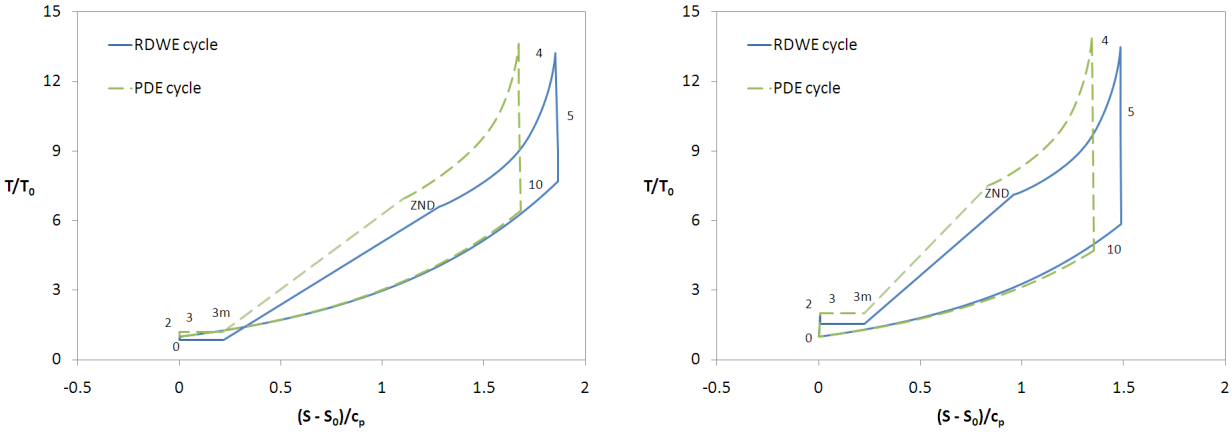

(a) $M_0 = 1.5$, $\Psi = 1.2$.

(b) $M_0 = 3.0$, $\Psi = 2.0$.

Figure 9. T–s diagram performance comparison between the steady-state RDWE and PDE models.

B. Component Analysis Using Exergy

As stated in the introduction, the second objective of the current work is to determine if the application of exergy analysis can assist with detonation-based engine cycle optimization. Using the same initial conditions as in Fig. 6(a), the exergy destruction for each component of the PDE model was calculated as a function of Ψ for $M_0 = 3.0$. The result is shown in Fig. 10(b) in a stacked diagram. The isentropic inlet and nozzle make no contribution to the exergy destruction. The exergy destruction due to mixing remains nearly constant as Ψ increases. However, the exergy destruction from the shock front of the detonation wave decreases significantly with Ψ. This trend is fairly difficult to notice with only a First Law-based analysis, but it should make physical sense. The entropy generation due to a normal shock is based on γ and the Mach number. As the temperature of the reactive mixture rises, the shock wave Mach number lowers both according to CJ theory and the local speed of sound before it. The exergy destruction caused by heat addition lowers with Ψ, but not significantly.

Figure 10(b) shows that the exergy destruction from the PDE continues to lower over the entire cycle static temperature ratio range. Such a conclusion was not reached in Fig. 6(a), where maximum performance occurred around $\Psi = 2.3$. This discrepancy between results is important as it shows that making this comparison is not correct. The exergy destruction charted only occurs inside the engine, so matching it with Eq. (9) leads to the discrepancy in the point of maximum performance. Instead, the internal exergy destruction can be matched only with the first two RHS terms, $(1 + f)\, Sa_{10} - Sa_0$. Figure 10(a) shows the normalized specific impulse trends calculated with only the stream thrust terms of Eq. (9) as well as the full equation. Using only the stream thrust terms, specific impulse continues to climb as exergy destruction minimizes. A full exergy analysis including the entropy generation from the wake of the engine must be utilized in order to show that $\Psi \approx 2.3$ is optimal for the engine. With the given information for these performance cases, the wake exergy generation can be found by using either a rate balance equation or a control volume analysis.[3,22] Equation (12) shows the exergy rate balance equation that can be written for the so-called flying engine with the entire specific thrust equation. Using this exergy rate balance equation shows that maximum performance indeed occurs at $\Psi \approx 2.3$.

$$\frac{F}{\dot{m}_0} V_0 = f\left(\frac{{V_0}^2}{2} + h_{PR}\right) - T_0\left(\dot{S}_{internal} - \dot{S}_{wake}\right) \tag{12}$$

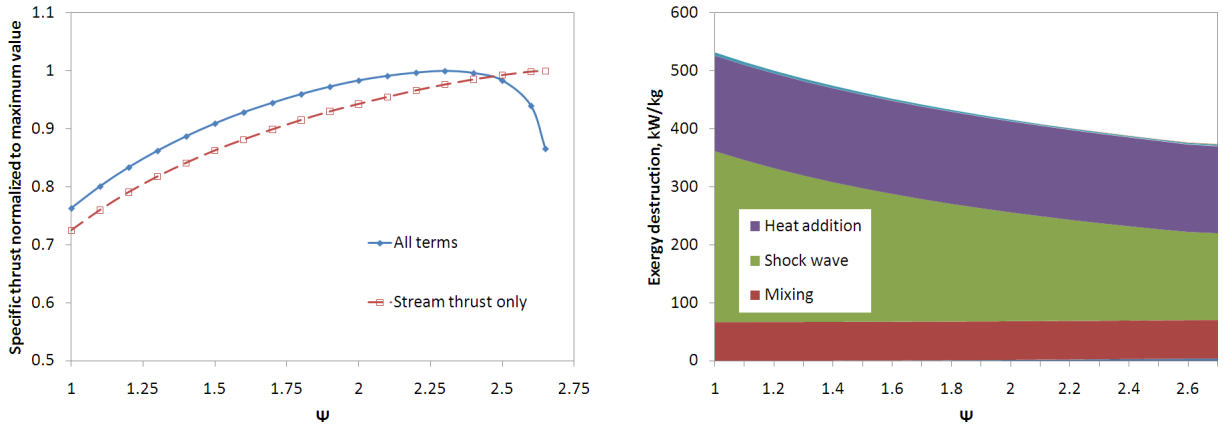

(a) Normalized specific thrust using part or all of Eq. (9).

(b) Rate of exergy destruction vs. Ψ.

Figure 10. PDE component exergy destruction trend comparison with specific thrust for an H_2–air engine at $M_0 = 3$, $q_0 = 95$ kN/m^2, and $T_0 = 216.7$ K.

Exergy analysis results for the RDWE using the same initial conditions are shown in Fig. 11. When the air expands isentropically into the detonation annulus of the RDWE to be mixed with the fuel, one must note that the loss in performance is not accounted for in terms of exergy destruction. The loss can be quantified by other means like thrust work potential.[4,5] While the decline in PDE exergy destruction appears to coincide with the increase in specific thrust, the loss of the RDWE thrust work potential causes its specific thrust to drop more rapidly than the rise in exergy destruction would indicate. Another interesting

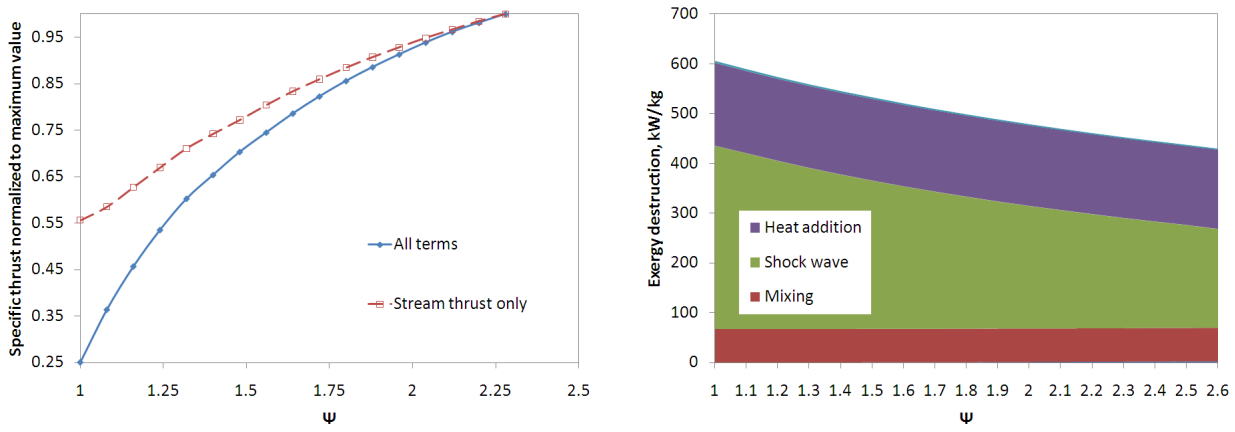

(a) Normalized specific thrust using part or all Eq. (9).

(b) Rate of exergy destruction vs. Ψ.

Figure 11. RDWE component exergy destruction trend comparison with specific thrust for an H_2–air engine at $M_0 = 3$, $q_0 = 95$ kN/m^2, and $T_0 = 216.7$ K.

trend related to the second purpose of this study is noticed between these exergy destruction calculations and the T–s diagrams of Fig. 9. For detonation-based engines, there exists an interrelationship between the inlet flow properties and the efficiency of the detonation wave. The CJ temperature and pressure ratios are generally higher as the initial temperature of the reactive mixture is reduced. Consequently, one might expect that lowering the reactive mixture temperature prior to the detonation wave would result in a performance increase. The difference in the entropy rise and exergy destruction for the shock wave, however, shows that the losses incurred as M_{CJ} increases with an inlet temperature reduction outweigh any benefit from an increase to the CJ ratios. This trend occurs even if the inlet pressure remains the same. Thus, both engines have optimal performance at the highest Ψ possible, unless the area ratio A_{10}/A_0 increases to the point where it significantly affects the specific thrust or the engine becomes unstable.

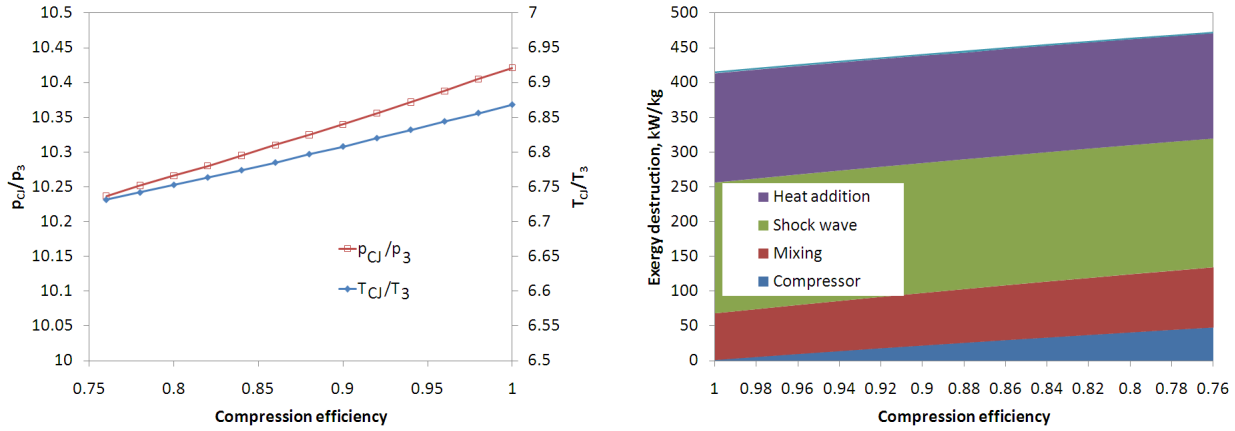

(a) Decline of CJ ratios vs. η_c.

(b) Rate of exergy destruction vs. η_c.

Figure 12. PDE component exergy destruction trend comparison including compression efficiency for an H_2–air engine at $M_0 = 3$, $q_0 = 95$ kN/m^2, $\Psi = 2.0$, and $T_0 = 216.7$ K.

Figure 12 shows another example of the exergy destruction calculations for the PDE of Fig. 10 with $\Psi = 2.0$ and the inclusion of the component efficiency metric η_c. Here, Fig. 12(a) shows the impact that η_c has on the CJ property ratios. As expected, the effect turns out to be relatively small since the value of η_c only affects the inlet pressure. Fig. 12(b) shows the exergy destruction as the First Law compression efficiency decreases. The data does in fact indicate some interrelationship effects. As η_c reduces, the shock wave and heat addition exergy destruction rates decrease from 157.1→151.8 kW/kg and 187.6→184.7 kW/kg, respectively. Of course,

the benefits are outweighed by the increase in compressor and mixing exergy destruction. Although these results are relatively minor, the example shows the kinds of results that can be obtained with the exergy analysis method, which presumably becomes more useful as complexities are added to the engine models.

V. Conclusions

A performance comparison between airbreathing PDE and RDWE models with steady state inlets and nozzles has been made. In terms of specific impulse and thrust, the PDE performs better at low supersonic flight speeds because the losses from the RDWE area expansion are relatively large. As M_0 increases, the performance between the engines gradually becomes comparable. The selection of one over another depends on which engine can operate near to these ideal model performance predictions as part of a practical design. PDEs benefit from their long history of research and development, where multi-tube engines with a common inlet appear feasible with current technology. Problems indicated by the steady state model include complexities related to mixing of the exhaust products, their interaction with a nozzle and refilling of the tubes, and the systems required to operate the tubes at high frequency. Sustainability of the detonation wave in a RDWE is a current problem, but the engine could benefit from a high energy density and less complexity with mixing of the exhaust.

A combined First and Second Law analysis for aerospace applications will probably be most beneficial for combined aircraft/engine/mission optimization approaches. However, accounting for entropy generation and exergy destruction with detonation-based engines leads to useful results in these models because the cycles have several sources of losses that can affect each other (perhaps more than a Brayton cycle engine because the CJ property ratios can vary with parameters like Ψ and η_c). The analyses in this study more clearly indicate the sources of losses in the engines. They also show how the different loss components can affect each other and add up to characterize the total engine performance.

Acknowledgments

Research into this subject for EMB was funded by a 2009 U.S. Air Force Research Laboratories summer internship (Air Vehicles Directorate, Design Analysis Methods Branch).

References

[1]Bejan, A., *Entropy Generation Minimization*, CRC Press, Boca Raton, FL, 1996.

[2]Moorhouse, D. J., "Proposed System-Level Multidisciplinary Analysis Technique Based on Exergy Methods," *Journal of Aircraft*, Vol. 40, No. 1, 2003, pp. 11–15.

[3]Riggins, D. W., Moorhouse, D. J., and Camberos, J. A., "Characterization of Aerospace Vehicle Performance and Mission Analysis Using Thermodynamic Availability," *Journal of Aircraft*, Vol. 47, No. 3, 2010, pp. 904–916.

[4]Roth, B., "Work Potential Perspective of Engine Component Performance," *Journal of Propulsion and Power*, Vol. 18, No. 6, 2002, pp. 1183–1190.

[5]Riggins, D. W., "Evaluation of Performance Loss Methods for High-Speed Engines and Engine Components," *Journal of Propulsion and Power*, Vol. 13, No. 2, 1997, pp. 296–304.

[6]Baker, M. L., Huang, J., Riggins, D. W., and Camberos, J. A., "Second-Law Methods for the Analysis & Design of Hypersonic Vehicles," *39th AIAA Thermophysics Conference*, AIAA 2007-4055, 2007.

[7]Doty, J. H., Camberos, J. A., and Moorhouse, D. J., "Benefits of Exergy-Based Analysis for Aerospace Engineering Applications: Part 1," *40th Thermophysics Conference*, AIAA 2008-4355, 2008.

[8]Doty, J. H., Camberos, J. A., and Moorhouse, D. J., "Benefits of Exergy-Based Analysis for Aerospace Engineering Applications: Part 2," *47th AIAA Aerospace Sciences Meeting*, AIAA 2009-1598, 2009.

[9]Braun, E. M., Lu, F. K., Wilson, D. R., and Camberos, J. A., "Airbreathing Rotating Detonation Wave Engine Cycle Analysis," *46th AIAA/ASME/SAE/ASEE Joint Propulsion Conference and Exhibit*, AIAA 2010-7039, 2010.

[10]Petela, R., "Application of Exergy Analysis to the Hydrodynamic Theory of Detonation in Gases," *Fuel Processing Technology*, Vol. 67, No. 2, 2000, pp. 131–145.

[11]Heiser, W. H. and Pratt, D. T., *Hypersonic Airbreathing Propulsion*, AIAA Education Series, Washington, DC, 1994.

[12]Goodwin, D., "Cantera: Object-Oriented Software for Reacting Flows," *http://code.google.com/p/cantera*, accessed June 30, 2009.

[13]Browne, S., Ziegler, J., and Shepherd, J. E., "Numerical Solution Methods for Shock and Detonation Jump Conditions," Tech. Rep. GALCIT Report FM2006.006, California Institute of Technology, Pasadena, CA, Aug. 2008.

[14]Bykovskii, F. A., Zhdan, S. A., and Vedernikov, E. F., "Continuous Spin Detonations," *Journal of Propulsion and Power*, Vol. 22, No. 6, 2006, pp. 1204–1216.

[15]Kailasanath, K., "Recent Developments in the Research on Pulse Detonation Engines," *AIAA Journal*, Vol. 41, No. 2, 2003, pp. 145–159.

[16]Wintenberger, E. and Shepherd, J. E., "Model for the Performance of Airbreathing Pulse-Detonation Engines," *Journal of Propulsion and Power*, Vol. 22, No. 3, 2006, pp. 593–603.

[17]Wu, Y., Ma, F., and Yang, V., "System Performance and Thermodynamic Cycle Analysis of Airbreathing Pulse-Detonation Engines," *Journal of Propulsion and Power*, Vol. 19, No. 4, 2003, pp. 556–567.

[18]Ma, F., Choi, J. Y., and Yang, V., "Thrust Chamber Dynamics and Propulsive Performance of Multitube Pulse Detonation Engines," *Journal of Propulsion and Power*, Vol. 21, No. 4, 2005, pp. 681–691.

[19]Heiser, W. H. and Pratt, D. T., "Thermodynamic Cycle Analysis of Pulse Detonation Engines," *Journal of Propulsion and Power*, Vol. 18, No. 1, 2002, pp. 68–76.

[20]Endo, T. and Fujiwara, T., "Analytical Estimation of Performance Parameters of an Ideal Pulse Detonation Engine," *Transactions of the Japan Society for Aeronautical and Space Sciences*, Vol. 45, No. 150, 2003, pp. 249–254.

[21]Bejan, A., *Advanced Engineering Thermodynamics*, John Wiley & Sons, Inc., New York, 1997.

[22]Riggins, D. W., Taylor, T., and Moorhouse, D. J., "Methodology for Performance Analysis of Aerospace Vehicles Using the Laws of Thermodynamics," *Journal of Aircraft*, Vol. 43, No. 4, 2006, pp. 953–963.